Simulation of capillary soil water flow under arid conditions: application to soil types in the Western Desert of Egypt

W.G.M. Bastiaanssen
M. Menenti
P. Kabat

Report 2

The WINAND STARING CENTRE, Wageningen (The Netherlands), 1990

ABSTRACT

Bastiaanssen, W.G.M., M. Menenti and P. Kabat, 1990. Simulation of capillary soil water flow under arid conditions: application to soil types in the Western Desert of Egypt. Wageningen (The Netherlands), The Winand Staring Centre. Report 2.
24 pp.; 5 figs.; 3 tables.

To predict the salinization due to the existence of shallow (saline) groundwater, factors affecting the capillary soil water flow must be properly described. Bare soil evaporation under arid conditions is characterized by vapour transport through the topsoil. The simulation of soil water flow under these conditions requires a coupling between the mechanisms of liquid, vapour and heat transport. A two-layer conceptual model has been developed by distinguishing an upper soil layer, where water flow takes place in the vapour phase and a lower soil layer where water flow takes place in the liquid phase. The depth of the interface depends on soil hydraulic properties. Core samples for determination of soil hydraulic properties were collected in the Western Desert of Egypt.
The rate of evaporation has been simulated using effective transport resistances above the evaporation front. The interrelation between soil type, depth of the evaporation front, the actual evaporation and the depth of the water table is demonstrated. It is shown that evaporation varies especially when the depth of the groundwater table is less than 70 cm below soil surface. The depth of the evaporation front may be a more precise decision criterion to prevent and locate salinization from capillary soil water flow than water table depth.

Keywords: salinization, liquid flow, vapour flow, evaporation front, water table, thermal conductivity, vapour diffusion.

ISSN 0924-3062

This report was published before as:
Bastiaanssen, W.G.M., M. Menenti and P. Kabat, 1990. Simulation of capillary soil water flow under arid conditions: application to soil types in the Western Desert of Egypt. In: Proceedings Symposium on Land Drainage for Salinity Control in Arid and Semi-Arid Regions. Cairo, February 25-March 2, 1990, Cairo, Egypt, Volume 2, p. 260-273.

The WINAND STARING CENTRE for Integrated Land, Soil and Water Research, Postbus 125, 6700 AC Wageningen (The Netherlands). Phone: +31 8370 19100; fax: +31 8370 24812; telex 75230 VISI-NL

The WINAND STARING CENTRE is continuing the research of: the Institute for Land and Water Management Research (ICW), Institute for Pesticide Research, Environment Division (IOB), Dorschkamp Research Institute for Forestry and Landscape Planning, Division of Landscape Planning (LB), and Soil Survey Institute (STIBOKA).

Project 370.3 [REP/2]

CONTENTS

1 INTRODUCTION

Problems arising from salinity control in arid and semiarid regions have caused an increased need of understanding the coupling between the terms of the groundwater balance i.e. recharge, evaporation and drainage. Salinization occurs through both shallow (saline) groundwater and inadequate leaching of irrigated lands (Smedema and Rycroft 1983). Salinization by the evaporation of water delivered by soil capillary flow, has been an underestimated subject especially about natural lowlands with subsurface inflow and (reclaimed) irrigated agricultural lands. The natural evaporation of groundwater recharge areas like old lands adjacent to reclaimed areas and natural depressions e.g. ancient oases and playas, have a peculiar effect on land salinization and regional water flow. The rate of upwards salt movement is proportional to the capillary soil water flux (mixing cell approach). The existance of a relationship between the vertical profile of salt concentration and evaporation processes in unsaturated soil has been demonstrated by means of experiments (e.g. Nakayama et al. 1973). It has been shown by Menenti (1984) that values of the depth of the evaporation front determined on the basis of salt concentration fit the general relationship between depth of the evaporation front and time, as observed by a variety of experimental techniques. The EVADES-model (Bastiaanssen et al. 1989) can be applied to describe the evolution of the depth of the evaporation front and, therefore, the depth of the salt accumulation, on the basis of convection of conservative solutes. The model has been validated with measurements collected during field experiments in the Qattara depression.

Water management for salinity control in all cases seeks for control of the water table, which should be lower than the so-called critical depth. Drainage is a solution to minimize the capillary rise of groundwater. Drainage criteria in this sence must be tuned with the characteristics of convective soil water flow through the unsaturated zone. To describe the impact of the depth of the water table on salinization more precisely soil water flow through the unsaturated soil must be properly simulated. The concentration of conservative solutes depends through the mixing cell approach on soil water content. During fallow periods, soils in arid regions dry out considerably. Soil water displacement under these conditions can not be estimated on the basis of liquid phase transport equations only. This requires for a coupling between the mechanisms for liquid, vapour and heat transport.

2 SOIL WATER TRANSFER PROCESSES UNDER ARID CONDITIONS

Bare soil evaporation is potential when the soil does not restrict liquid flow. The evaporation then is based upon meteorological conditions only. At low soil water contents, the ability of the soil to conduct water in the liquid phase is low; the liquid diffusivity becomes less than the vapour diffusivity (Jackson 1964). So a two-phase flow with vapour transport in the topsoil and liquid transport in the subsoil must be accounted for. Preliminary, a definition of the liquid-vapour interface i.e. evaporation front must be briefly recalled (Menenti 1984). Gas diffusion in partly water filled pores as described by Fick's law (Equation 1) remains only valid in pores having a radius (r_m) much larger than the mean free path of a water vapour molecule (l_m). Fick's diffusion only applies for circumstances where large number of gas-gas collisions takes place:

$$q_v = - D_v \frac{\partial \rho_v}{\partial z} \qquad (kg.m^{-2}.s^{-1}) \qquad (1)$$

In much smaller pores, ($r_m << l_m$), Fick's diffusion velocity is exceeded by the velocity of Knudsen flow. So there will be a rapid phase transition at a specific matric pressure head, from a condition where pores with $r_m > l_m$ are water filled to the case of pores with $r_m < l_m$ being air filled. This process will give a sharp transition of soil water content with depth. The critical pore size for Knudsen flow coincides with the mean free path of water vapour.

The particular matric pressure head (h_m) where $r_m = l_m$ can be calculated on the basis of cylindrical capillaries:

$$h_{me} = \frac{1}{\rho_w g} \frac{2\sigma_{wa}}{l_m} \qquad (m) \qquad (2)$$

The related soil water content (θ_e) can be found from the soil water retention characteristic i.e. $h_m(\theta)$ relationship. The depth of the evaporation front (z_e) can be traced as that $\theta(z) = \theta_e$. Different water transfer processes occur simultaneously and affect the actual flux rate (Kabat 1986; Ten Berghe 1986). The driving forces are dynamical and mutually related. The following transport processes must be systematically addressed:

* liquid flow ($r_m > l_m$)
  - by gradient of soil moisture content (matric-liquid forces)
  - by gradient of soil temperature (liquid-thermal forces)
  - by gradient of solute concentration (liquid-solute forces)

* vapour flow ($r_m > l_m$)
  - by gradient of vapour density (matric-vapour forces
  - by gradient of soil temperature (vapour-thermal forces
  - by gradient of solute concentration (vapour-solute forces)
* vapour flow ($r_m < l_m$)
  - by gradient of pressure head (viscous forces)

The contributive set of equations are presented in table 1. Very small pressure gradients can produce viscous Knudsen fluxes that exceeds diffusive Fickian fluxes (Thorstenson and Pollock 1989). Thermal convection enhances the conductive soil heat flow. The existence of convective flow above the evaporation front can be anticipated on the basis of soil temperature measurements. Several dynamic gradients and corresponding permeabilities are mutually related (Passerat de Silans et al. 1989). This especially holds true with large soil temperature gradients in the toplayer.

A pitfall applying to the quantification of the soil permeability to conduct water should be mentioned. The issue of the determination of transport coefficients constitutes a drawback of most studies towards capillary rise. Transport coefficients are hardly quantitatively measurable and not sharply defined. In this paper, a solution with 'effective soil resistance values' above the evaporation front will be presented.

Table 1 Governing water transport equations under arid conditions

Soil water flow process	Flux equation	Type of diffusivity
Isothermal isosaline liquid flow	$q_{l1} = -D_l(\theta)\frac{\partial\theta}{\partial z} - k(\theta)$	$D_l(\theta) = k(\theta)[\frac{\partial h_m}{\partial\theta}]_{T,C}$ (isothermal liquid diffusivity)
Isothermal saline liquid flow	$q_{l2} = -D_l(C)\frac{\partial C}{\partial z} + q_{l1}$	$D_l(C) = k(\theta,C)\,[\frac{\partial h_m + \partial h_{osm}}{\partial C}]_{\theta,T}$
Thermal isosaline liquid flow	$q_{l3} = -D_l(T)\frac{\partial T}{\partial z} + q_{l1}$	$D_l(T) = k(\theta,T)[\frac{\partial h_m}{\partial T}]_{\theta,C}$ (thermal liquid diffusivity)
Thermal saline liquid flow	$q_{l4} = q_{l3} + q_{l2} - q_{l1}$	
Isothermal isosaline vapour flow	$q_{v1} = -D_v(\theta)\frac{\partial\theta}{\partial z}$	$D_v(\theta) = D_v[\frac{\partial\rho_v}{\partial\theta}]_{T,C}$ or $D_v(\theta) = D_v[\rho_v sat\,\frac{\partial U}{\partial\theta}]_{T,C}$ (isothermal vapour diffusivity)
Isothermal saline vapour flow	$q_{v2} = -D_v(C)\frac{\partial C}{\partial z} + q_{v1}$	$D_v(C) = D_v[\frac{\partial\rho_v}{\partial C}]_{\theta,T}$ or $D_v(C) = D_v[U\frac{\partial\rho_v sat}{\partial C} + \rho_v sat\,\frac{\partial U}{\partial C}]_{\theta,T}$
Thermal isosaline vapour flow	$q_{v3} = -D_v(T)\frac{\partial T}{\partial z} + q_{v1}$	$D_v(T) = D_v[\frac{\partial\rho_v}{\partial T}]_{\theta,C}$ (thermal vapour diffusivity) $D_v(T) = D_v[U\frac{\partial_v sat}{\partial T} + \rho_v sat\,\frac{\partial U}{\partial T}]_{\theta,C}$
Thermal saline vapour flow	$q_{v4} = q_{v3} + q_{v2} - q_{v1}$	
Thermal convective flow	$q_{v5} = -\rho_v(\theta,T,C)V_{ca}$	

3 CONCEPTUAL MODEL: EFFECTIVE SOIL RESISTANCE FACTORS TO HEAT AND VAPOUR FLOW

The linkage between transport processes in the unsaturated zone and effective soil resistance factors can now be discussed. The soil transport resistance factors are an expression for the conductance of heat (R_{sh}) and vapour (R_{sv}) between the evaporation front and the soil surface. Further, R_{sh} and R_{sv} as valid for the soil above the evaporation front are related to the depth of the evaporation front (z_e). Theory of potential evaporation (with $R_{sv} = 0$ and $R_{sh} = 0$) applies with a zero depth of the evaporation front (fig. 1).

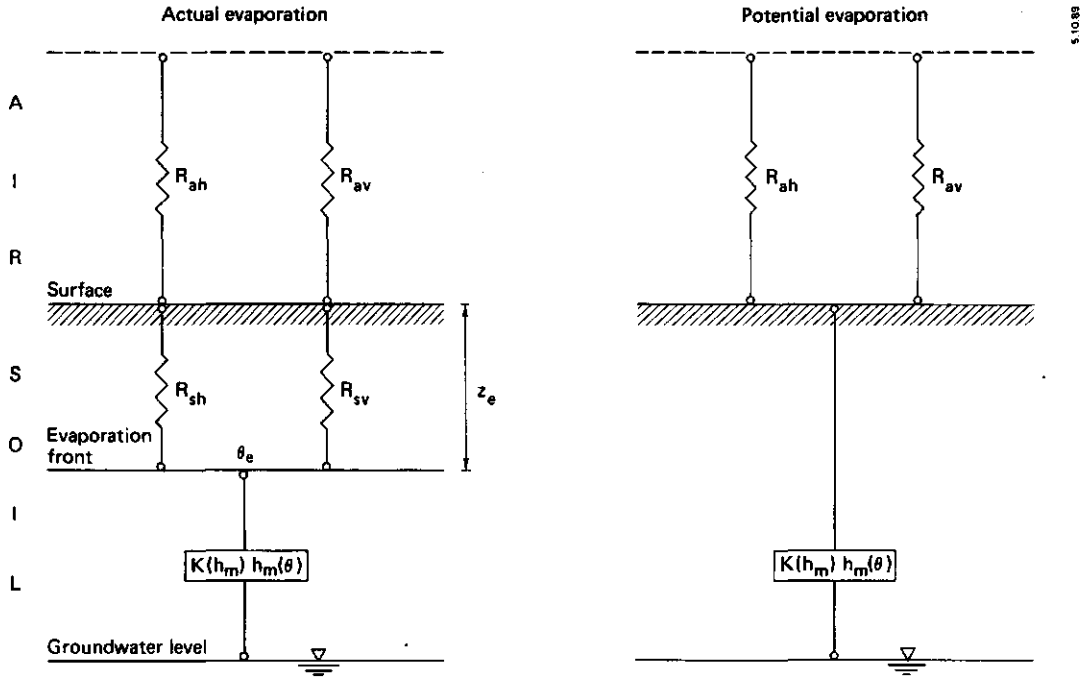

Fig. 1 Schematic representation of the resistance (R) to heat (h) and vapour (v) flow in air (a) and soil (s). The depth of the evaporation front (z_e) depends on the soil moisture contribution in the profile. Potential bare soil evaporation occurs when the limit of the depth of the evaporation front equals zero.

Their applicability in transport and combination equations for actual evaporation will be demonstrated now. The heat wave penetrating from the soil surface to the evaporation front can be written in terms of a flux as follows:

$$G_0 = -\lambda' \frac{T_0 - T_e}{z_e} = \frac{T_e - T_0}{R_{sh}} \qquad (W.m^{-2}) \qquad (3)$$

so $R_{sh} = z_e/\lambda'$ $\quad (W^{-1}.m^2.K)$ (4)

The transport of latent heat between the evaporation front and the soil surface reads:

$$LE = - \frac{\rho_a C_p}{\gamma R_{sv}} [e(T_e) - e(T_0)] \quad (W.m^{-2}) \tag{5}$$

The relative humidity of moist soil air at the evaporation front is nearly hundred percent, so that the actual vapour pressure at depth z_e with temperature T_e will approaches saturation. The direction of the fluxes presented, depends on the time of the day. It should be realized that upwelling vapour transport contrasts with downwelling heat transport during heating of the topsoil. Combination of the depicted transport equations through soil and transport equations through air, involving the concept of balancing in- and outgoing surface energy fluxes, yields a new combination equation for actual bare soil evaporation of the Penman-Monteith type (Menenti 1984).

4 SOIL PHYSICAL INTERPRETATION OF THE SOIL RESISTANCE FACTORS FOR HEAT AND VAPOUR TRANSPORT

A soil physical interpretation of R_{sh} and R_{sv} can be given on the basis of the transport processes mentioned in table 1.
Schematically, three cases in the topsoil can be thought of:

A) evaporation takes place at the soil surface with dominantly liquid flow (potential evaporation);
B) evaporation takes place inside the soil with Fickian vapour diffusion between the evaporation front and the soil surface (actual evaporation);
C) evaporation takes place inside the soil with thermal or free convection of moist air, between the evaporation front and the soil surface (actual evaporation).

Case A: When the evaporation site is at surface level, the limit of the depth of the evaporation front equals zero ($z_e = 0$). Pores are predominantly filled with water ($\theta > \theta_e$). Liquid displacement is the main transport process. Hence, there is no resistance for transport between the phase transition zone and the evaporation site.

$$\lim_{z_e \to 0} (LE_{act}) = LE_{pot} \tag{6}$$

$$R_{sh} = 0 \qquad (W^{-1}.m^2.K) \tag{7}$$

$$R_{sv} = 0 \qquad (s.m^{-1}) \tag{8}$$

Case B: In this case, the liquid transport capacity above the evaporation front ($\theta < \theta_e$) is limited. Density driven thermal and iso-thermal vapour diffusion can be lumped into an 'effective' molecular diffusion coefficient of water vapour in moist soil air ($D_v$eff). The latter can be written as an ordinary Fick-type equation for the soil layer between the evaporation front and the soil surface:

$$q_v = -D_v\text{eff}\,\frac{\delta\rho_v}{z_e} \quad \text{or} \quad = \frac{\delta\rho_v}{R_{sv}} \qquad (kg.m^{-2}.s^{-1}) \tag{9}$$

so

$$R_{sv} = z_e/D_v\text{eff} \qquad (s.m^{-1}) \tag{10}$$

The apparent soil thermal conductivity (λ') takes into account the overall effect of heat conduction and heat convection by mass flow. This parameter is quite relevant since the energy required for internal soil evaporation is released by the soil heat flow penetrating the soil surface (G_0). The resistance for the transport of heat in soil as derived from equation (3) reads as follows:

$$R_{sh} = z_e/\lambda' \qquad (W^{-1}.m^2.K) \tag{11}$$

Case C: Thermal convection of moist soil air occurs when temperature gradients cause air movement. A rule of thumb is that thermal or free convection will certainly occur when the air flow velocity becomes larger than two orders of magnitude the speed of vapour diffusion i.e. faster than $2.5\ 10^{-3}$ $m.s^{-1}$. Onset of thermal convection is likely when the Rayleigh number is higher than a treshold value of the Rayleigh number, depending on boundary conditions. Vapour flux, then can be expressed in the following form (see also table 1):

$$q_v = -\rho_v V_{ca} \qquad (kg.m^{-2}.s^{-1}) \tag{12}$$

To establish in this case a physical explanation of R_{sv}, the effective vapour diffusivity again is introduced ($D_v eff$). For the sake of simplicity, the convective soil air motion can be rearranged into an ordinary Fickian diffusion type equation:

$$-\rho_v V_{ca} = -D_v eff \frac{\delta \rho_v}{z_e} \qquad (kg.m^{-2}.s^{-1}) \tag{13}$$

To obtain the flow velocity (V_{ca}), a practical solution was found by considering the enhancement of conductive heat flow λ^* by thermal convection:

$$\lambda' = \lambda^* + \rho_a C_p V_{ca} \delta z \qquad (W.m^{-1}.K^{-1}) \tag{14}$$

Taking the limit of $V_{ca} = 0$ i.e. no moist air movement, λ' and λ^* are identical. The preceding discussion around λ' (case B) is identical for case C. Hence:

$$R_{sh} = z_e/\lambda' \qquad (W^{-1}.m^2.K) \tag{15}$$

$$R_{sv} = z_e/D_v eff \qquad (s.m^{-1}) \tag{16}$$

5 SIMULATION MODEL

A new finite difference one-dimensional numerical simulation model with thermal forcing for bare soil EVAporation in DESerts (EVADES) has been developed (Bastiaanssen et al. 1989). The EVADES-model contains the Richards equation for movement of water in the liquid phase Richards 1931; Feddes et al. 1988). At the evaporation front, a vapour continuity equation with 'effective' properties of the Fick-type is applied.

Resistance factors for the transport of vapour (R_{sv}) and heat (R_{sh}) are computed by means of the simulation of a moving evaporation front. The actual evaporation rate away from the surface is calculated by using Menenti's combination equation (Menenti 1984). The crucial role of apparent soil thermal conduction (λ') and effective vapour diffusivity ($D_v$eff) has already been stressed.

To apply equation (14), soil temperature should be listed as a standard meteorological observation parameter at stations. Values of λ' can then be gathered from the apparent thermal diffusivity. The speed of air movement (V_{ca}) is computed by applying equation (14), when λ^* is estimated from the composition of the different soil constituents. Soil temperature, as well air temperature, relative humidity, windspeed and net radiation were measured on

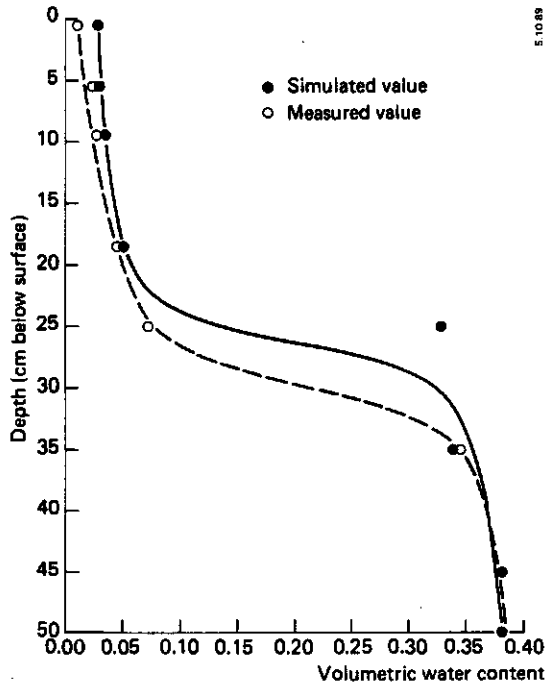

Fig. 2 Comparison between measured and simulated values of soil water content for a bare coarse sand profile as present at Bir Tarfawi in the Southwestern part of Egypt.

the spot at several localities during 1986-1988. Likewise, soil physical data were collected. Validation of equation (14) can be done by comparing the derived $D_v$eff-values through equation (13) with $D_v$eff-values obtained by inverse computation of Menenti's combination equaton with known actual evaporation values from field registrations (Bowen-ratio energy balance method). The outcome of comparisons between evaporation figures measured by the Bowen-ratio energy balance method and simulated evaporation rates by the EVADES-model were satisfactory (Bastiaanssen et al. 1989). The simulation results were verified against measurements of soil moisture content and soil temperature. The agreement was good (fig. 2). Figure 2 implies that the highest concentration of Na^- and Cl^- ions are found in the layer between 0-25 cm. To quantify the mass flux under the evaporation front (q_l), transport coefficients in the liquid phase for different soils have to be analysed separately.

6 CLASSIFICATION OF SOIL HYDRAULIC PROPERTIES

Liquid flow is the dominant transport process below the evaporation front. The soil dependent interaction between solid matrix and liquid is regulating the capacity of the soil to conduct water. So the upward liquid flux depends on soil dependent $h_m(\theta)$ and $K(h_m)$ relationships (see table 1). The depth of the evaporation front may be conceived as the locality where the drying power of the topsoil and the liquid transport capacity of the lower soil are in equilibrium. Hence, the depth of the evaporation front is aptly affected by the transport coefficients in the liquid phase.

In order to simulate the upward mass flux for various soil types, it was deemed necessary to develop a classification procedure for soils on a regional scale with different hydraulic properties. First of all, some 35 core samples were collected in and around the Qattara depression. The analysis of their individual trends were done at the soil physical laboratory at The Winand Staring Centre. A classification into groups with common properties was carried out. To identify groups with common properties, an analytical fit of the individual curves was initially undertaken using the S-shape of the Van Genuchten model (Van Genuchten et al. 1988). This allows for a better interpolation between the dotted data points, obtained from tensiometers. The Van Genuchten model consists of six parameters. By clustering the six parameters of the individual $h_m(\theta)$ and $K(h_m)$ curves, six soil groups could be identified. The cluster analysis was done with both a complete linkage and Ward technique. Respectively the squared euclidean distance and euclidean distance method was applied. The values of the six Van Genuchten parameters for each group are presented in table 2.

Table 2 Mean Van Genuchten parameters for identified soils in the Qattara depression, Western Desert of Egypt. For the explanation of the symbols applied, one is referred to the work of Van Genuchten et al. (1988).

Group	Brief description	θ_r	θ_s	α	n	l	k_{sat}
		($cm^3.cm^{-3}$)	($cm^3.cm^{-3}$)	(cm^{-1})	(-)	(-)	($cm.d^{-1}$)
1	sand, sandy puffy	0.043	0.347	0.022	2.130	-1.369	0.963
2	loam, clay, hummocky	0.135	0 340	0.030	2.086	-1.344	2.068
3	coarse sand, puffy	0.000	0.358	0.031	1.670	-2.252	0.569
4	porous puffy	0.221	0.473	0.009	2.021	-0.508	1.123
5	porous clayey puffy	0.000	0.496	0.120	1.219	-6.482	9.122
6	fine sandy puffy	0.017	0.348	0.046	1.453	-1.162	16.081

The shape of the $h_m(\theta)$ relation of the identified groups provides information on the texture (grain size distribution) and salinity. A high residual water content (θ_r) (group 2,4) in all cases seems to be correlated with a high salinity. Enhancement of the matric pressure head by osmotic forces is obvious with lower water content i.e. a higher concentration of solutes. Group 3 shows the typical matric-liquid interactions for dune sand formations, widely present in the Western Desert.

7 RESULTS AND DISCUSSION

The salts were dominantly of the NaCl type. The highest observed salt concentration in hummocky topsoils was 5.5 mol.l^{-1}! The effective transport resistances (R_{sv}, R_{sh}) were independently from the mass flow, using soil temperature measurements, estimated. Since the simulated and measured evaporation are nearly identical, theories presented with equation (14) hold true. The variation of the apparent soil thermal conductivity is marginal (λ' = 0.3-0.7 W.m^{-1}.K^{-1}). The effective vapour diffusivity shows more variation, namely between 0.1-6.0 10^{-3} m^2.s^{-1}. Latter can be considered as a soil resistance for vapour transport as presented in figure 3.

R_{sv}-values are lower during the summer period. This can be explained on basis of the enhancement of heat flow by the thermal convection of moist soil air, which increases the effective vapour diffusivity. The differentiation between group 1 and group 3 depends on the unsaturated hydraulic conductivity. The effect of the soil hydraulic properties on the locality of the evaporation front is depicted in figure 4.

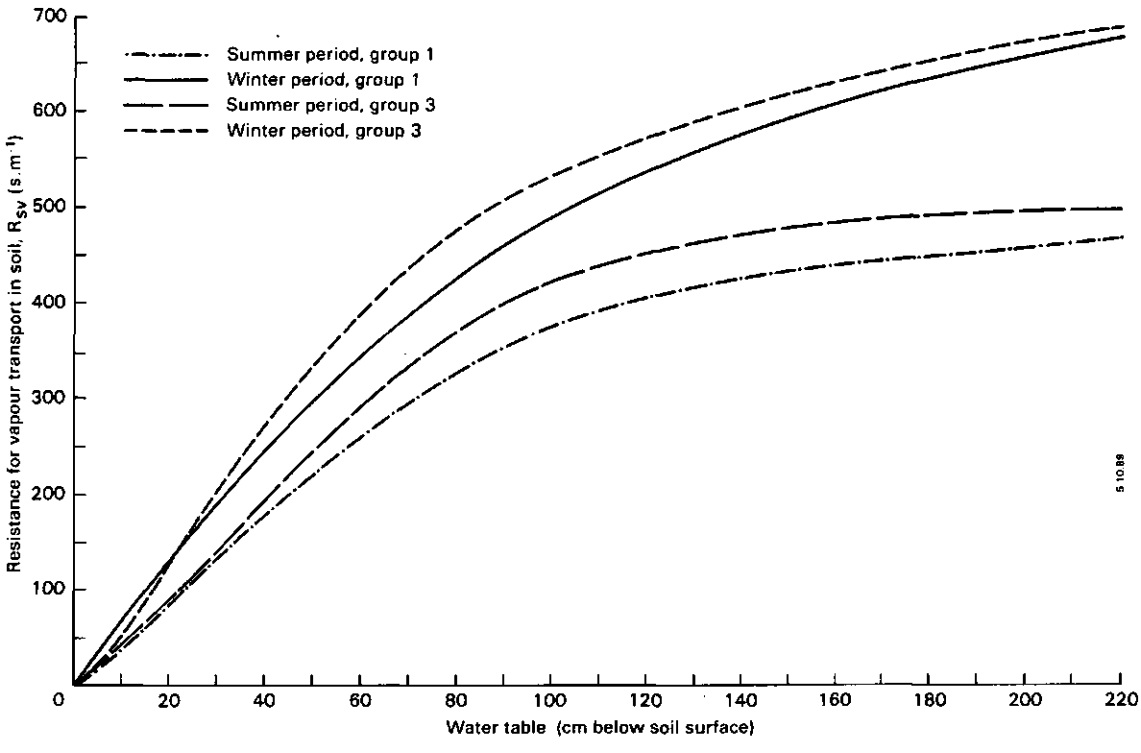

Fig. 3 The resistance for vapour transport in soil as a function of water table and soil type. Two identified soil types according the classification procedure are considered (group 1, 3 - Western Desert of Egypt - table 2). Soil types are classified on the basis of their hydraulic properties using cluster analysis techniques.

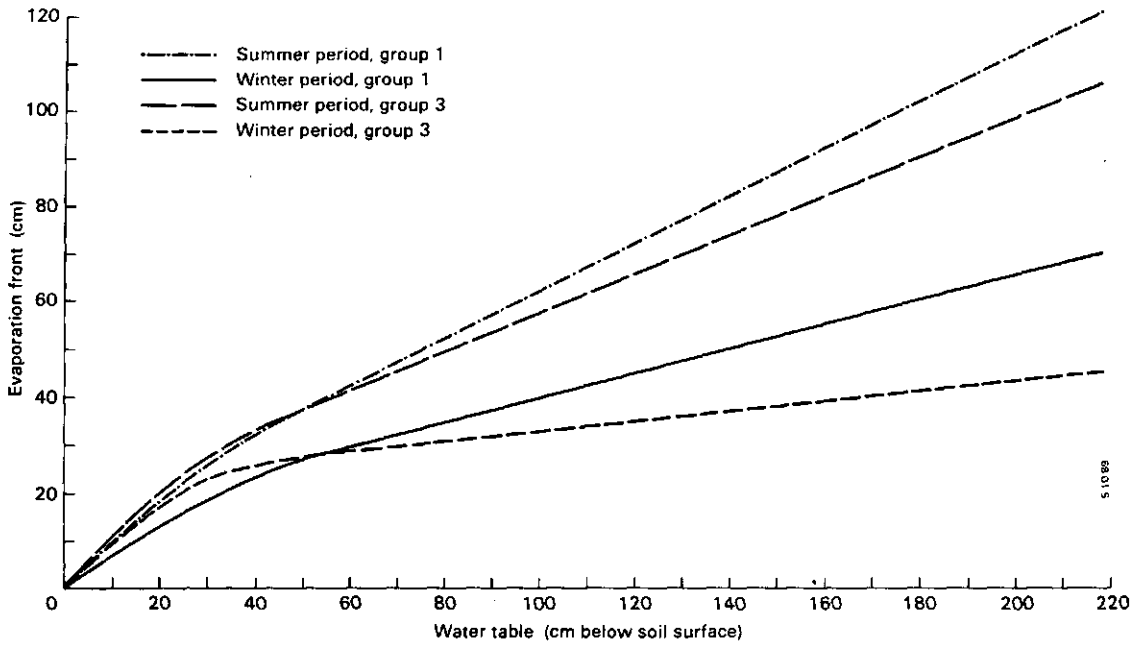

Fig. 4 The locality of the evaporation front in relation with the water table for two soil types (group 1, 3) in the Western Desert of Egypt. The soil types of figure 3 are considered, both for the summer and winter season.

The impact of the atmospheric drying power on soil wetness is more evident during the hot season. Finally, the relation between water table, depth of the evaporation front and actual evaporation was worked out for the hydraulic classes presented. Three sections in the curve presented in figure 5 can be distinguished:

(i) the steep part of the curve is governed by meteorological conditions;
(ii) the transition zone is highly sensitive to the water table depth;
(iii) the flat part of the curve is fully controlled by the soil capillary properties.

The weather impact on the evaporation is especially evident with low soil resistance values i.e. the evaporation front close to the soil surface. This is the case with very shallow groundwater as present in playas or on lands after irrigation. Then the evaporation varies mainly with surface reflectance (table 3). This feature is less evident during the winter, since the incoming shortwave radiation is much less. High soil resistance values, with deeper water tables, result in low evaporation values with minor seasonal effects. Evaporation then depends on soil properties like specific permeability and transport coefficients. Interpretation of daily evaporation throughout the whole year can be intuitively obtained from the annual air temperature or solar radiation cycle.

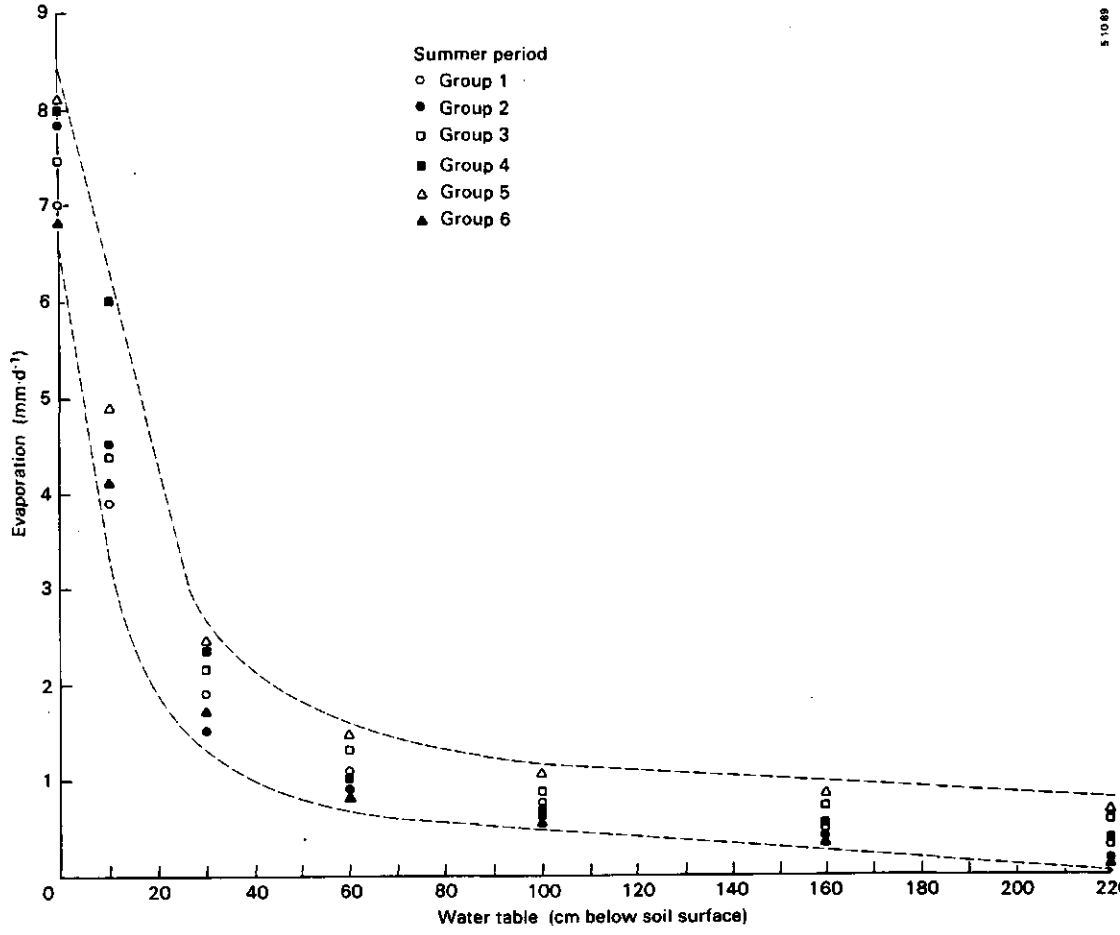

Fig. 5 Evaporation of six classified soil types in the Western Desert of Egypt in relation with the water table. Only the summer period is considered.

Table 3 Seasonal variation of potential and actual evaporation (water table 200 cm below soil surface) for six classified soil types in the Western Desert of Egypt

Group	Normalized surface reflectance (-)	E_{pot} summer ($mm.d^{-1}$)	E_{pot} winter ($mm.d^{-1}$)	Specific permeability (m^2)	E_{act} summer ($mm.d^{-1}$)	E_{act} winter ($mm.d^{-1}$)
1	0.30	6.98	4.05	0.105 10-14	0.35	0.33
2	0.18	7.88	4.53	0.296 10-14	0.29	0.22
3	0.25	7.48	4.31	0.725 10-15	0.63	0.24
4	0.17	7.96	4.58	0.159 10-14	0.44	0.35
5	0.19	8.08	4.65	0.109 10-13	0.73	0.19
6	0.30	6.99	4.04	0.212 10-13	0.28	0.22

8 CONCLUSIONS

To prevent evaporation from groundwater for salinity control in arid and semiarid regions, evaporation from capillary rise should be reduced to a minimum. A proper description of capillary water flow requires knowledge of multi-phase flow under hot and saline conditions. The depth of the evaporation front, depends on the transport coefficients of liquid flow ($k(h_m)$). Simulation of transient soil water flow under arid conditions is hampered by the knowledge of the transport coefficients. A cluster analysis of the Van Genuchten parameters of individual $h_m(\theta)$ and $k(h_m)$ relationships is a handy tool to classify and reduce the variation of hydraulic properties. Transport coefficients for water in the vapour phase can be rewritten as soil 'effective' properties and can be verified with field observations.

The weather impact on the evaporation rate especially is noticeable with the existence of a shallow evaporation front e.g. playa's and overirrigated areas. The actual evaporation rate rapidly decreases with a water table deeper than 70 cm below soil surface. The evaporation linearily decreases with water tables deeper than 70 cm.

Management of the water table in arid and semiarid areas should consider the evaporation zone. This allows for an improved estimation of the actual mass flux to the topsoil, the salinization by conservative solutes and the locality of precipitated salts.

REFERENCES

Bastiaanssen, W.G.M., P. Kabat and M. Menenti, 1989. A new simulation model of bare soil evaporation in deserts, EVADES. ICW-note 1938, The Winand Staring Centre for Integrated Land, Soil and Water Research, Wageningen, The Netherlands, 73 pp.

Berghe, H.F.M., ten, 1986. Heat and water transfer at the bare soil surface. Ph.D. Thesis, Agricultural University, Wageningen, The Netherlands, 214 pp.

Feddes, R.A., P. Kabat, P.J.T. van Bakel, J.J.B. Bronswijk and J. Halbertsma, 1988. Modelling soil water dynamics in the unsaturated zone - state of the art. Journal of Hydrology 100: 69-111.

Genuchten, M.Th. van, F. Kaveh, W.B. Russel and S.R. Yates, 1988. Direct and indirect methods for estimating the hydraulic properties of unsaturated soils. In: Bouma, J. and A.K. Bregt (eds.). Proc. Int. Symp. on Land Qualities in Space and Time: 61-72, PUDOC, Wageningen, The Netherlands.

Jackson, R.D., 1964. Water vapour diffusion in relative dry soil. Soil Sci. Soc. Am. Proc. 28(2): 172-176; 28(4): 464-470.

Kabat, P., 1986. Moisture, heat and salt dynamics in fields with trickler and localized irrigation. Thesis, Technical University, Prague, Czechoslovakia, 115 pp.

Menenti, M., 1984. Physical aspects and determination of evaporation in deserts applying remote sensing techniques. Ph.D. thesis/ ICW Report 10, The Winand Staring Centre for Integrated Land, Soil and Water Research, Wageningen, The Netherlands, 202 pp.

Nakayama, F.S., R.D. Jackson, B.A. Kimball and R.J. Reginato, 1973. Diurnal soil water evaporation: chloride movement and accumulation near the soil surface. Soil Sci. Soc. Amer. Proc. 37: 509-513.

Passerat de Silans, A., L. Bruckler, J.L. Thony and M. Vauclin, 1989. Numerical modeling of coupled heat and water flows during drying in a stratified bare soil - comparison with field observations. Journal of Hydrology 105: 109-138.

Richards, L.A., 1931. Capillary conduction of liquids through porous mediums. Physics 1: 318-333.

Smedema, L.K. and D.W. Rycroft, 1983. Land drainage: planning and design of agricultural drainage systems. Cornell University Press, New York, USA, 370 pp.

Thorstenson, D.C. and D.W. Pollock, 1989. Gas transport in unsaturated zones; multicomponent systems and the adequacy of Fick's laws. Water Resources Research 25,3: 477-507.

NOMENCLATURE

Symbol	Interpretation	Units
C	solute concentration	$mol.l^{-1}$
C_p	air specific heat at constant pressure	$J.kg^{-1}.K^{-1}$
D_l	liquid diffusivity	$m^2.s^{-1}$
D_v	vapour diffusivity	$m^2.s^{-1}$
$D_v eff$	effective vapour diffusivity	$m^2.s^{-1}$
e	vapour pressure	mbar
E_{act}	actual evaporation	$m.d^{-1}$
E_{pot}	potential evaporation	$m.d^{-1}$
g	gravitational constant	$m.s^{-2}$
G_0	soil heat flux	$W.m^{-2}$
h	heat	-
h_m	matric pressure head	m
h_{me}	matric pressure head at the evaporation front	m
H	sensible heat flux	$W.m^{-2}$
k_{sat}	saturated hydraulic conductivity	$m.s^{-1}$
$k(h_m)$	unsaturated hydraulic conductivity	$m.s^{-1}$
$k(\theta)$	unsaturated hydraulic conductivity	$m.s^{-1}$
l	empirical constant van Genuchten-model	-
l_m	mean molecular free path of water vapour	m
LE	latent heat flux	$W.m^{-2}$
LE_{act}	actual latent heat flux	$W.m^{-2}$
LE_{pot}	potential latent heat flux	$W.m^{-2}$
n	empirical constant van Genuchten-model	-
q_l	liquid flux	$m.s^{-1}$
q_v	vapour flux	$kg.m^{-2}.s^{-1}$
R_{ah}	resistance for heat transport in air	$s.m^{-1}$
R_{av}	resistance for vapour transport in air	$s.m^{-1}$
r_m	pore radius	m
R_{sh}	resistance for heat transport in soil	$s.m^{-1}$
R_{sv}	resistance for vapour transport in soil	$s.m^{-1}$
T	soil temperature	K
T_e	soil temperature at the evaporation front	K
T_0	surface temperature	K
U	relative humidity	-
V_{ca}	convective air flow velocity	$m.s^{-1}$
z	depth	m
z_e	depth of the evaporation front	m
α	empirical constant Van Genuchten-model	m^{-1}
ρ_a	air density	$kg.m^{-3}$
ρ_v	vapour density	$kg.m^{-3}$
$\rho_v sat$	saturated vapour pressure	-
ρ_w	water density	$kg.m^{-3}$
θ	soil water content	$m^3.m^{-3}$
θ_e	soil water content at the evaporation front	$m^3.m^{-3}$
θ_r	residual soil water content	$m^3.m^{-3}$
θ_s	saturated soil water content	$m^3.m^{-3}$
λ'	apparent soil thermal conductivity	$W.m^{-1}.K^{-1}$
λ^*	effective soil thermal conductivity	$W.m^{-1}.K^{-1}$
σ_{wa}	surface tension of water against air	$N.m^{-1}$
γ	psychrometric constant	$mbar.K^{-1}$